

# Consideration of the transient material behavior under variable amplitude loading in the fatigue assessment of nodular cast iron using the strain-life approach

Jan Hesseler | Jörg Baumgartner  | Christoph Bleicher

Materials and Components, Fraunhofer Institute for Structural Durability and System Reliability LBF, Darmstadt, Germany

## Correspondence

Jörg Baumgartner, Materials and Components, Fraunhofer Institute for Structural Durability and System Reliability LBF, Darmstadt, Germany.  
Email: joerg.baumgartner@lbf.fraunhofer.de

## Funding information

German Federal Ministry of Economics Affairs and Energy (BMWi), Grant/Award Number: 0325707

## Abstract

The consideration of realistic load assumptions is important for the fatigue design of highly stressed nodular cast iron components for wind energy application. Especially in case of overloads causing elastic–plastic deformation, residual stresses may have a strong impact on fatigue life. In strain-controlled fatigue tests with constant and variable amplitudes, the influence of overloads on lifetime was investigated. During fatigue testing, the transient material behavior, cyclic hardening, cyclic relaxation of the residual stresses, and quasi-static creep effects of the EN-GJS-400-18-LT was recorded and evaluated. To quantify the influence of the transient material behavior on the calculated lifetime, fatigue analyses are carried out with the strain-life approach, both with and without consideration of the transient material behavior. The results show that conservative damage sums are derived if the transient material behavior, especially the relaxation of tensile residual stresses, is neglected.

## KEYWORDS

nodular cast iron, overload, strain-life approach, transient material behavior, variable amplitude loading, wind energy

## 1 | INTRODUCTION

Nodular cast iron components are often used in the wind energy sector due to their high design freedom and high load capacity. Highly stressed components, such as the rotor hub or the main frame, are typically made of nodular cast iron (GJS).

Due to stochastic wind loads,<sup>1</sup> variable amplitude loads are used for the fatigue assessment. Numerous fatigue approaches are available for the assessment of components.<sup>2</sup>

In industrial application, guidelines with stress-based approaches are frequently used.<sup>3,4</sup> These consider influences due to, for example, stress gradients (microstructural

support effects), surface roughness, or temperature. The loads are usually represented by a load spectrum transformed to a load ratio of  $R = -1$  by a given mean stress sensitivity. In this way, a fatigue assessment can be quickly performed for complex parts with variable amplitude loading. But, due to the assumed linear-elastic material behavior, sequence effects are not taken into account.

However, high operating loads or overloads, for example, caused by storms or grid losses, which lead to plastic deformation of the material and thus to residual stresses, cannot be evaluated directly with stress-life approaches. Furthermore, stress-based approaches do not take sequence effects into account. Subsequently, no changes of residual stresses

This is an open access article under the terms of the Creative Commons Attribution License, which permits use, distribution and reproduction in any medium, provided the original work is properly cited.

© 2021 The Authors. *Fatigue & Fracture of Engineering Materials & Structures* published by John Wiley & Sons Ltd.

due to, for example, exceedance of the yield stress can be considered. In addition, the stress-life approaches generally only cover the high cycle fatigue range ( $N > 10^4$ ) and cannot assess damage components for overload cycles in the low cycle fatigue (LCF) regime.

The strain-life approach, as described, for example, Dowling<sup>5</sup> or in the FKM guideline,<sup>6</sup> can be applied in an acceptable calculation time to evaluate the fatigue life for crack initiation. It uses the cyclically stabilized material behavior and does not consider transient effects, for example, creep or cyclic mean stress relaxation. However, it can consider changes of the residual stresses due to exceedance of the yield stress and also allows the evaluation of load cycles in the LCF regime. Subsequently, the strain-life approach has been often used to evaluate the fatigue strength of components with overloads in the load spectrum.

The fatigue strength of welded joints with tensile overloads was analyzed in various publication.<sup>7,8</sup> The applied overload leads to compressive residual stresses in the fatigue critical weld toe notch and subsequently to an increase in fatigue life. With the strain-life approach, the beneficial effects could be quantified. However, if an overload is applied that leads to tensile residual stresses in the fatigue critical locations, harmful effects need to be considered. The fatigue strength of case-hardened specimens in strain-controlled tests was investigated.<sup>9</sup> Due to periodic compressive overloads, the endurable strain amplitudes are significantly lowered due to the relaxation of compressive residual stresses.

Besides the influence of the overload on the crack initiation life, the residual stress state has also an influence on the crack propagation life. Tensile residual stresses lead to an accelerated crack propagation, compressive one to a retardation of the crack growth.<sup>7,10</sup>

Independent from the sign of the residual stresses, that is, high tensile or high compressive ones, these can partially be reduced by the subsequent load cycles. This can be explained on one hand by an exceedance of the yield stress as it is covered by the strain-life approach. On the other hand, the residual stresses can be changed by a cyclic mean stress relaxation<sup>11</sup> or static creep.<sup>12</sup> With material models,<sup>13</sup> these transient effects can be partially described. Due to their complexity and computing time, however, they are seldomly used in industrial application.

In cast iron, process-related material defects often cannot be avoided. The influence of those defects on fatigue strength of nodular cast iron is investigated.<sup>14–20</sup> In this paper, the focus of the investigations is to determine the influence of the transient material behavior on the calculated damage sum. The influence of defects on fatigue properties was not investigated in this work; therefore, specimens containing major discontinuities were not considered in the evaluation. Moreover, large castings are not easy to be inspected with

non-destructive testing during the production process. Especially shrinkages with size of 1 mm or less cannot be detected when looking at components with wall-thicknesses over 200 mm. In this case, the material has to be treated as sound even so smaller defects might be present. All defects still occurring less than 1 mm are within the scatter band and need to be taken as “as cast.” More detailed information on the microstructure of the specimens is presented in another publication.<sup>21</sup>

In this work, the influence of the transient material behavior on the calculated lifetime is investigated. For this purpose, strain-controlled fatigue tests and fatigue analyses with the strain-life approach were carried out. The specimens for the strain controlled fatigue test were taken from a machine frame of a wind energy turbine and tested under constant and variable amplitude loading.<sup>21</sup> To investigate the influence of overloads on lifetime, three different scenarios were investigated: (a) without overload, (b) with an overload at the beginning, and (c) with an overload after one transit of the load spectrum ( $L_S = 5 \cdot 10^5$ ). The overload consists of a cycle in the compression range ( $\Delta\varepsilon = 1\%$ ,  $R_\varepsilon = -\infty$ ) and was selected in such a way that it leads to high tensile residual stresses.

## 2 | FATIGUE TESTS

### 2.1 | Specimen for the fatigue test

For the fatigue tests, unnotched specimens of EN-GJS-400-18-LT were used, which were taken from a main frame of a wind turbine. The position of the main frame where the specimens have been taken had a wall thickness of approx.  $t = 85$  mm. In the test volume, the specimens have a diameter of  $d = 15$  mm and a length of  $l = 25$  mm (Figure 1). The highly stressed volume<sup>22,23</sup> of the specimen is  $HBV_{90\%} = 6.122$  mm<sup>3</sup>. It should be noted that  $HBV_{90\%}$  is not only in the test volume but also extends into the transition radius. The chemical composition is shown in Table 1. Static tests showed a tensile strength  $R_m = 363.2$  MPa, a yield strength  $R_{p0.2} = 225$  MPa, and a breaking strain of  $A_5 = 26.6\%$ .

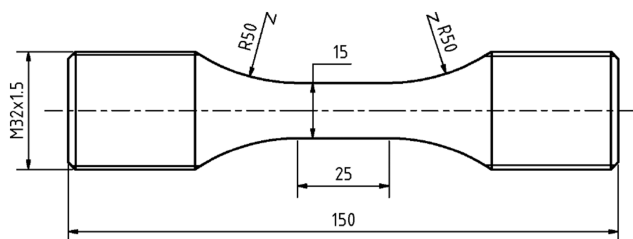


FIGURE 1 Geometry of the specimen used for the investigations

Metallurgical investigations<sup>21</sup> showed a nodularity of 85.3 and a fraction of ferrite/pearlite/graphite of 82.2/4.6/13.3. Additional information is given in another publication.<sup>20</sup>

## 2.2 | Fatigue test under constant amplitude loading

The strain controlled tests were carried out at room temperature on a servo-hydraulic test rig with test frequencies between  $f=0.1$  and 20 Hz and a strain ratio of  $R_\epsilon = -1$  in orientation to ISO 12106.<sup>24</sup> The first 10 load cycles were always performed at a frequency  $f=0.1$  Hz. Then, in order to reduce the test duration, the frequency was increased as a function of the load levels. The tests were run until crack initiation. The crack initiation was detected by a stiffness decrease of the specimen. Based on the measured strain and the force on the specimen, a decrease of stiffness of 20% related to the initial state was used to detect the crack initiation. During the tests, the forces resp. nominal stresses were continuously recorded with a rate of 200 data points per cycle.

The number of cycles to crack initiation  $N_i$  and the elastic-plastic material behavior were determined

according to ISO 12106.<sup>24</sup> The stress-strain curve<sup>25</sup> in the description according to (1) and the strain-life curve<sup>26-29</sup> according to (2) are shown in Figure 2.

$$\epsilon_a = \epsilon_{a,e} + \epsilon_{a,p} = \frac{\sigma_a}{E} + \left(\frac{\sigma_a}{K'}\right)^{\frac{1}{n'}} \quad (1)$$

$$\epsilon_a = \epsilon_{a,p} + \epsilon_{a,p} = \frac{\sigma_f'}{E} \cdot (2 \cdot N)^b + \epsilon_f' \cdot (2 \cdot N)^c \quad (2)$$

The parameters of the strain-life curve,  $\epsilon_f'$  (fatigue ductility coefficient),  $\sigma_f'$  (fatigue strength coefficient),  $b$  (fatigue strength exponent), and  $c$  (fatigue ductility exponent), shown in Table 2, are determined with a linear regression in double logarithmic  $\epsilon_{el}-N$  space and double logarithmic  $\epsilon_{pl}-N$  space. The parameters of the stress-strain curve,  $K'$  (strength coefficient), and  $n'$  (strain hardening) are determined by the compatibility conditions<sup>30</sup>:

$$n' = \frac{b}{c} \quad (3)$$

$$K' = \frac{\sigma_f'}{\left(\epsilon_f'\right)^{n'}} \quad (4)$$

TABLE 1 Chemical compositions of the investigated cast iron alloy EN-GJS-400-18-LT in %

C	Si	Mn	P	S	Mg	Cu	Ni
3.75	2.16	0.21	0.022	0.005	0.041	0.010	0.02

The fatigue tests under constant amplitude loading show cyclic hardening, that is, an increase in the stress amplitude at a constant strain amplitude (Figure 3). This cyclic hardening is dependent on the strain level. At low

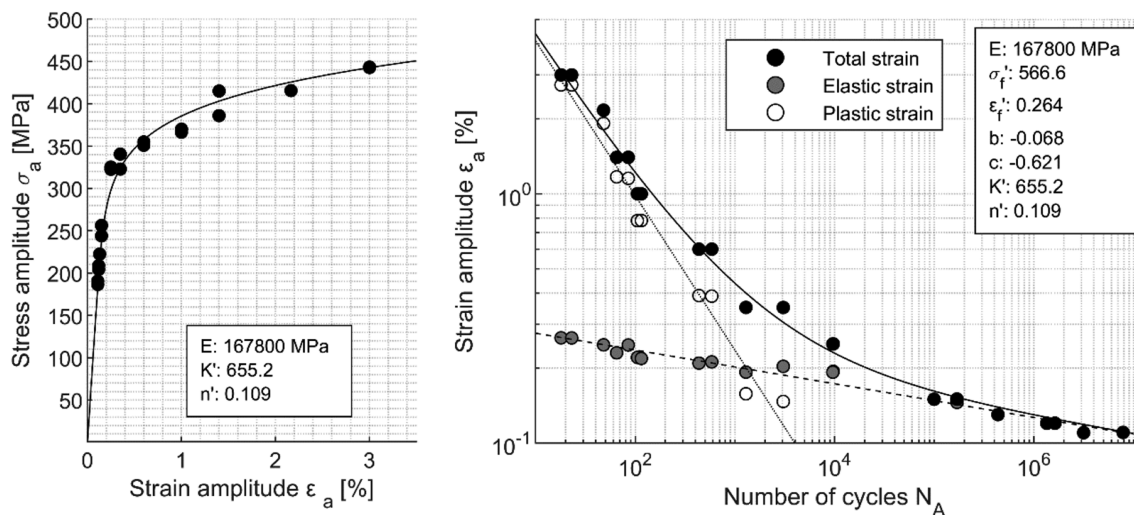


FIGURE 2 Cyclic stress-strain curve and strain-life curve for EN-GJS-400-18-LT

TABLE 2 Parameter of the strain-life curve and cyclic stress-strain curve for EN-GJS-400-18-LT

Material	$E$ (MPa)	$\sigma_f'$ (MPa)	$\epsilon_f'$	$b$	$c$	$K'$	$n'$
EN-GJS-400-18-LT	167,800	567	0.264	-0.068	-0.621	655.2	0.109

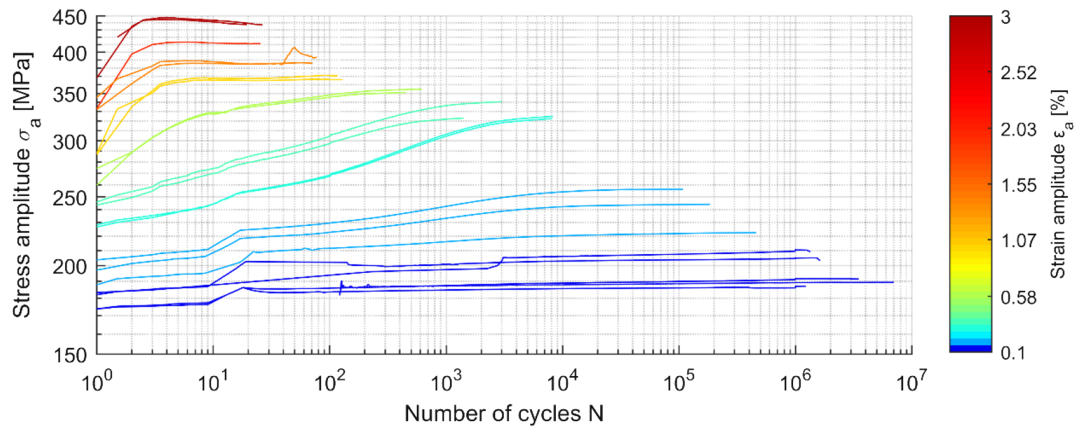


FIGURE 3 Stress amplitude in strain-controlled tests showing cyclic hardening until crack initiation [Colour figure can be viewed at wileyonlinelibrary.com]

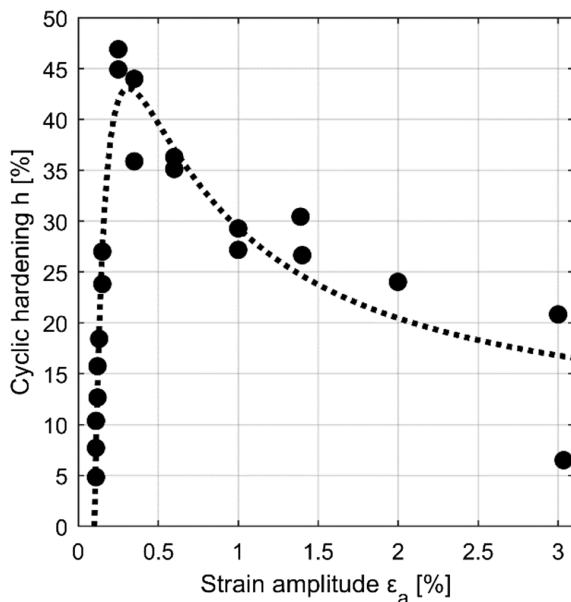


FIGURE 4 Cyclic hardening depending on the strain amplitude

strain levels, the material shows only a low cyclic hardening. The maximum cyclic hardening is achieved at a strain amplitude of about  $\epsilon_a = 0.25\%$ . Higher strain amplitudes show a lower relative cyclic hardening, probably induced by a starting crack initiation, which leads to a decrease of the stress amplitude (Figure 4). The strain hardening  $h$  is defined according to (5), where  $N_i$  represents the number of cycles to crack initiation.

$$h = \frac{\max(\sigma_{a,N=1..N_i})}{\sigma_{a,N=1}} - 1 \quad (5)$$

The increase of the test frequency after 10 cycles leads to an increase of the stress amplitude. This is most obvious

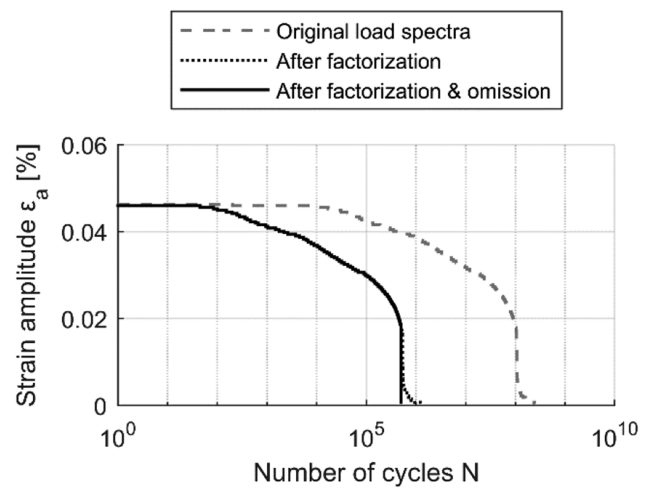


FIGURE 5 Load spectrum

in tests with low strain amplitudes, where the frequency difference between the first 10 cycles and the following cycles is highest.

### 2.3 | Fatigue test under variable amplitude loading

The fatigue tests with variable strain amplitude were performed on the same servo-hydraulic test rig as those with constant strain amplitudes. In order to use realistic loads in the investigations, a load spectrum derived from a wind turbine<sup>21</sup> was used that corresponds to a life of 20 years and has a strain ratio of  $R_e = -1$ .

In order to obtain a suitable load-time history for the fatigue tests, the load spectrum is reduced from  $L_S = 2.8 \cdot 10^8$  cycles to  $L_S = 5 \cdot 10^5$  cycles by means of factorization and omission (Figure 5). This is necessary because the



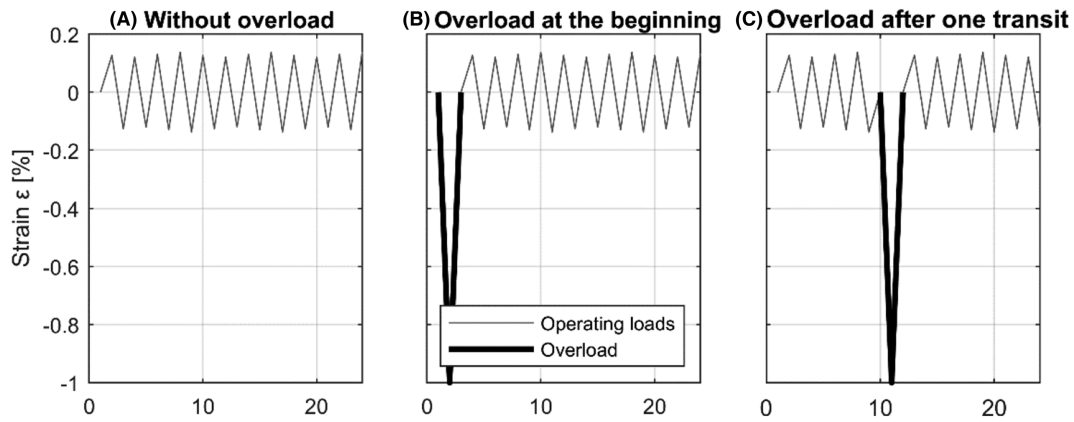


FIGURE 6 Load time history with and without overload

load-time history should be run through several times in Gaßner tests.<sup>31</sup>

In order to investigate the influence of an overload on the lifetime, three load scenarios were investigated (Figure 6):

- a. without overload
- b. with an overload at the beginning
- c. with an overload after one transit, that is, after  $L_S = 5 \cdot 10^5$  cycles

The overload at the beginning is expected to have a large influence on lifetime, since the material has not yet achieved cyclic hardening. Therefore, a higher degree of yielding is expected than with the cyclically stabilized material after  $L_S$  cycles. The purpose of the overload after one transit is to check the influence of the time of occurrence and whether the overload has a minor influence on lifetime due to the cyclic hardening of the material. The overload was selected in such a way that high residual tensile stresses are generated, which have a negative effect on lifetime. However, the overload should not cause any significant damage. The overload therefore consists of one load cycle with a strain range of  $\Delta\epsilon = 1\%$  in compression direction.

The Gaßner-curves show a partially significant influence of the overload on the fatigue life (Figure 7). This is highest at low strain amplitudes since the residual stresses due to the overload are not reduced due to the subsequent load cycles. The local yield stress is never exceeded. At high strain amplitudes, the influence of the overload decreases since a partly relaxation of the residual stresses occurs. This leads to different slopes of the Gaßner-curves and a coincidence of the curves at about  $N = 5 \cdot 10^5$  cycles. This is caused by a reduction of the residual stress at high strain levels. In the Gaßner-curves,

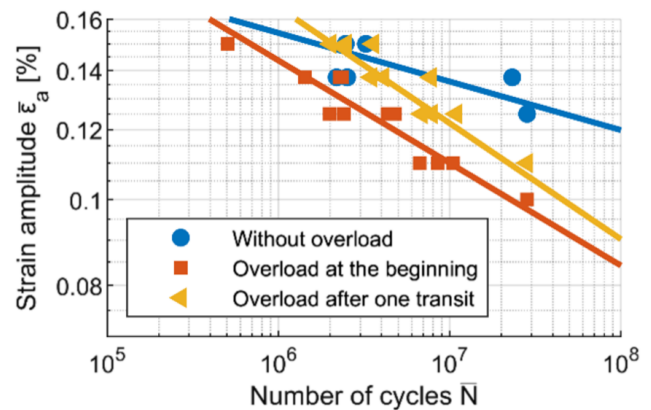


FIGURE 7 Gaßner curves under variable amplitude loading with and without overload [Colour figure can be viewed at wileyonlinelibrary.com]

following number of tests could be considered in the evaluation: without overload: 6, overload at the beginning: 12, and overload after one transit: 10.

## 2.4 | Changes in the local mean respectively residual stresses

The work distinguishes between the following influences:

1. cyclic relaxation of local mean stress
2. static creep
3. change of local mean stress by exceeding the yield limit

All three phenomena are connected to each other and have a high influence on the residual stress state at high loads with plastic strains. A schematic representation can be seen in Figure 8.

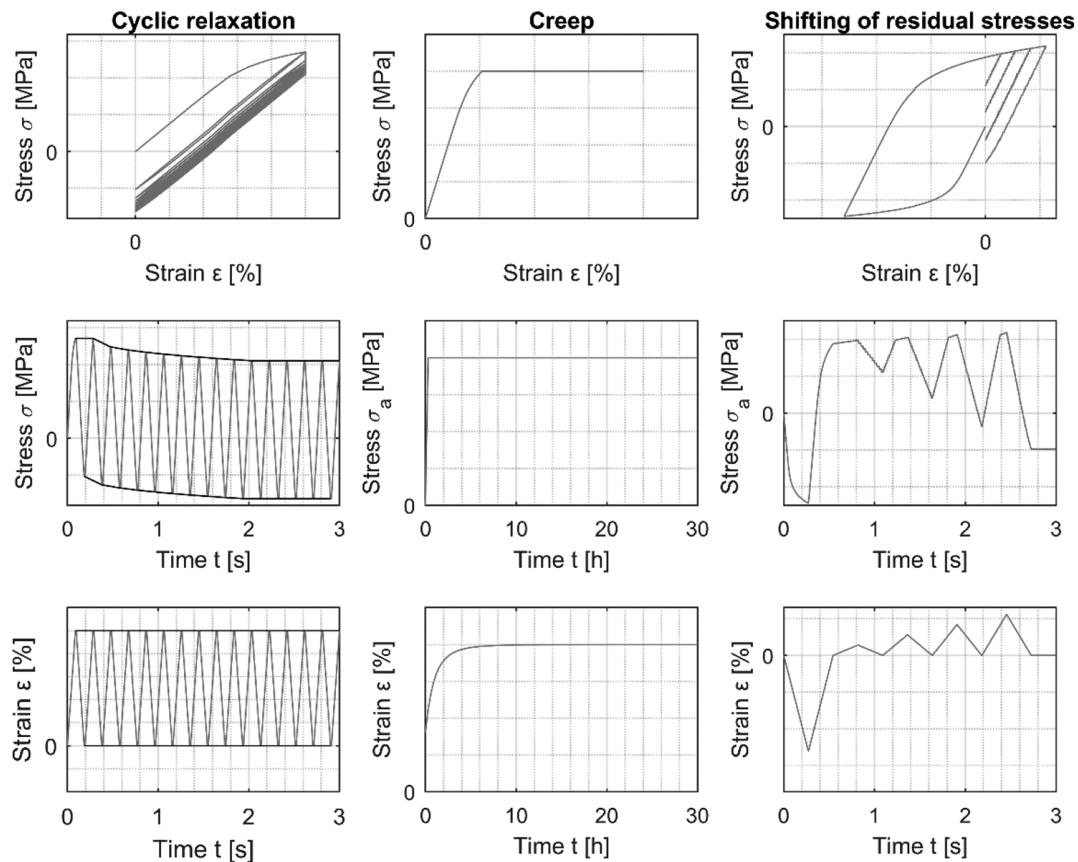


FIGURE 8 Schematic representation of different phenomena to change local mean resp. residual stresses

1. Cyclic relaxation is defined as decrease in the residual stress state (local mean stress) under constant strain-controlled testing<sup>11</sup> ( $\epsilon_m \neq 0$ ).
2. Static creep is defined as an increase in plastic elongation at constant stress ( $\sigma_m \neq 0$ ). This effect can also be identified for an EN-GJS-400-15.<sup>12</sup>
3. Residual stress reduction by exceeding the yield limit means that if the yield limit is exceeded, the residual stresses can be reduced or, depending on the load level, built up in the opposite direction.<sup>32,33</sup>

All effects are addressed when loading with significant plastic strains and a stress ratio of  $R \neq -1$ . The significance of the individual influences depends on the load-time-history.

### 3 | FATIGUE ANALYSIS

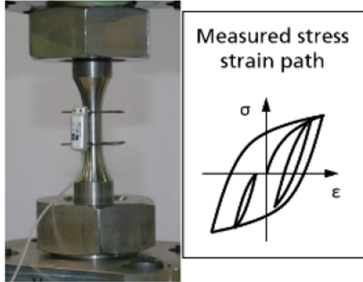
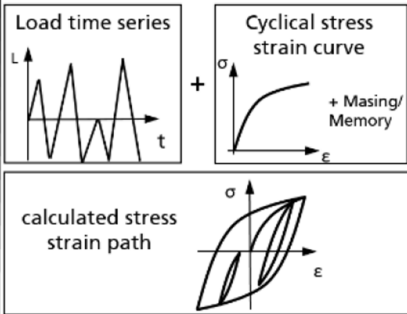
#### 3.1 | Applied fatigue assessment approaches

When the strain-life approach is applied in industrial application, no transient material behavior is generally

used in the fatigue assessment. Effects such as cyclic hardening or cyclic mean stress relaxation are not considered. A cyclically stabilized stress-strain behavior over the entire component lifetime is usually assumed. As it can be seen in Figure 3, the EN-GJS-400-18-LT, however, shows a load-dependent hardening. A stabilization of the stresses at a constant strain level does not take place. The hardening takes place continuously until failure.

To investigate the influence of the transient material behavior on the damage sum, two different damage calculations are carried out for the fatigue tests with variable amplitude loading (Figure 9). Input data for both approaches are the recorded strain-time course from the fatigue tests and the strain-life curve from the constant amplitude fatigue tests. In the first variant, the fatigue assessment is considering the transient material behavior, and the recorded stress amplitudes have been used. Subsequently, all transient effects are covered. This variant is referred to as the experimental variant in the following. In the second variant, the fatigue assessment is carried out without consideration of transient material effects, and the stress amplitudes were numerically derived based on the cyclically stabilized material behavior. This approach is common and often used when elastic-plastic

FIGURE 9 Approaches for the fatigue assessments: 1. Experimental variant and 2. Numerical variant [Colour figure can be viewed at wileyonlinelibrary.com]

	1. Fatigue assessment with transient material behaviour (experimental)	2. Fatigue assessment w/o transient material behaviour (numerical)
Material behaviour	Transient material behaviour <ul style="list-style-type: none"> <li>• Cyclic hardening</li> <li>• Cyclic mean stress relaxation</li> <li>• Creep</li> </ul>	Cyclically stabilized material behaviour <ul style="list-style-type: none"> <li>• No cyclic hardening</li> <li>• Cyclic mean stress relaxation</li> <li>• No creep</li> </ul>
Stress strain path		
Damage calculation	<ol style="list-style-type: none"> <li>1. Cycle counting</li> <li>2. Mean stress correction</li> <li>3. Linear damage accumulation</li> </ol>	<ol style="list-style-type: none"> <li>1. Cycle counting</li> <li>2. Mean stress correction</li> <li>3. Linear damage accumulation</li> </ol>

stresses have to be evaluated, and it is referred to as the numerical variant in the following.

Since the Wöhler-curve and the Gaßner-curves were derived with the same unnotched specimen with a low surface roughness ( $R_Z < 6.3 \mu\text{m}$ ), no support effects or surface influences need to be taken into account. The HCM<sup>33</sup> cycle counting algorithm was used to identify closed hysteresis. The mean stress was considered using the damage parameter  $P_B$ <sup>34</sup> (6) that is closely related to  $P_{SWT}$ .<sup>35</sup>  $P_B$  was used because it is easy to apply and it has the ability to control the mean stress sensitivity.

$$P_B = \sqrt{(\sigma_a + \sigma_m \cdot k) \cdot \epsilon_a \cdot E} \quad (6)$$

The parameter  $k$  (7) was used to consider the desired mean stress sensitivity.<sup>6</sup>

$$k = \begin{cases} M \cdot (M + 2) & \text{in case } \sigma_m \geq 0 \\ \frac{M}{3} \cdot \left(\frac{M}{3} + 2\right) & \text{in case } \sigma_m < 0 \end{cases} \quad (7)$$

Different recommendations for mean stress sensitivities can be found in literature. According to the FKM guideline,<sup>4</sup> a mean stress sensitivity of  $M = 0.21$  is calculated for the EN-GJS-400-18-LT. However, a mean stress sensitivity of  $M = 0.5$  is determined in fatigue test for EN-

GJS-400-18-LT<sup>36</sup> and is used in the present fatigue analysis.

Next to  $P_{SWT}$  and  $P_B$ , there exist numerous other damage parameters, such as  $P_J$ .<sup>6</sup> However, these are more complex in their application and not widely used in industrial application.

In order to visualize the influence of the mean stress sensitivity within the  $P_B$  parameter, stress amplitudes were adjusted to derive constant  $P_B$ -values at different mean stresses. Figure 10 shows examples of stress amplitudes and mean stresses for four different  $P_B$ -values. It can be observed that the slope of the curves at high mean tensile stresses is flatter at low  $P_B$ -values than at high ones. This means that the mean stress sensitivity depends on the load level.

The linear damage accumulation according Palmgren<sup>37</sup> and Miner<sup>38</sup> was used to calculate the damage sum. The two fatigue assessments differ only with regard to the stress behavior that occurs due to the measured strain-time history in the fatigue test.

### 3.2 | Derived stresses for fatigue assessments

In the experimental variant, the transient material behavior is taken into account in the fatigue assessment. For this purpose, the actual strain from the extensometer and

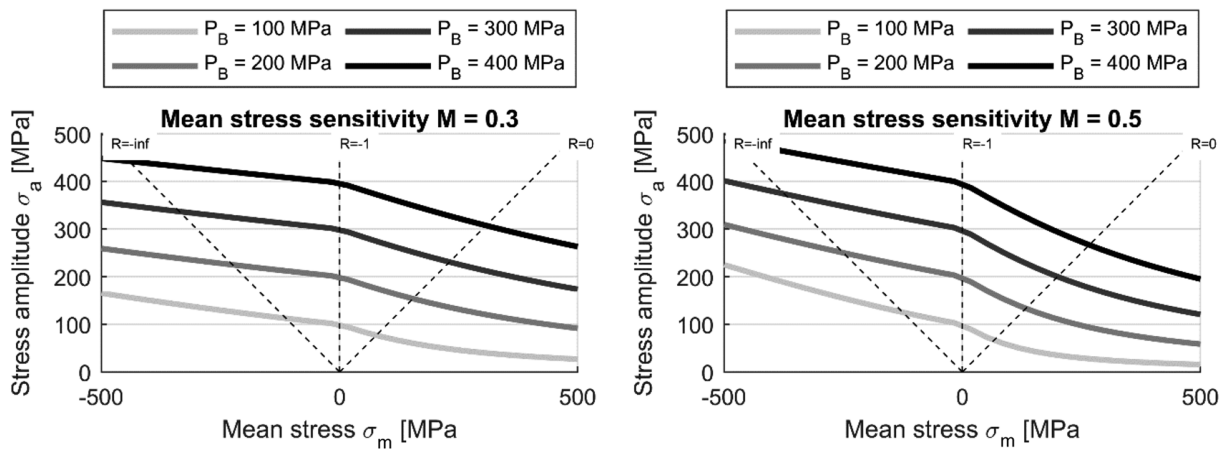


FIGURE 10 Haigh-diagram for constant  $P_B$ -values and two different mean stress sensitivities

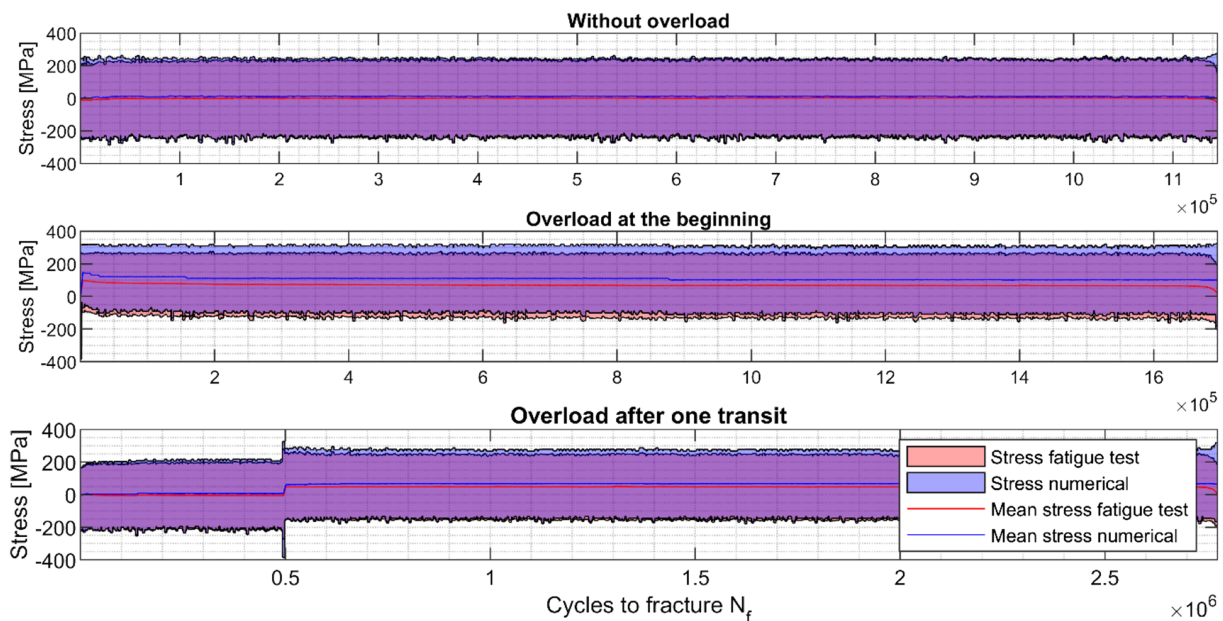


FIGURE 11 Calculated and measured mean stresses in the variable amplitude loading tests [Colour figure can be viewed at [wileyonlinelibrary.com](http://wileyonlinelibrary.com)]

the actual force were recorded during the Gaßner tests. Based on the force, the nominal stress was calculated. Thus, no model of the stress–strain behavior was necessary in the damage calculation since the real measured time-dependent stress–strain behavior was used. This includes cyclic hardening, cyclic mean stress relaxation, and creep.

In the numerical variant, the corresponding stress is calculated on the basis of the actual strain with the cyclically stabilized material behavior and the Masing-Memory model.<sup>32,33</sup> The Masing-Memory model considers the shift of residual stresses caused by exceeding the yield stress, but does not consider cyclic hardening, cyclic mean stress relaxation, or creep.

The two variants are based on the identical strain-time history; only the underlying stress history is different due to the material behavior. A comparison of the stress curves is shown in Figure 11. In the scenario without overload, a deviation of the maximum stress can be seen at the beginning of the test. This is due to the not yet cyclically hardened stress–strain behavior of the transient material behavior. In the further course the deviations of the stresses are small but constant.

The compressive overload lead to measured residual stresses of  $\sigma_{res,exp} = 260$  MPa and calculated residual stresses of  $\sigma_{res,num} = 320$  MPa, independent of the time at which the overload occurs. These residual stresses were reduced by the following loads: in the



scenario with overload at the beginning, the calculated stresses are significantly higher than the stresses derived based on the transient material behavior ( $\sigma_{m,exp} = 68$  MPa vs.  $\sigma_{m,num} = 103$  MPa). In the scenario with overload after one transit, the calculated mean stresses are also higher than the measured ones ( $\sigma_{m,exp} = 49$  MPa vs.  $\sigma_{m,num} = 67$  MPa).

In the second variant with numerically derived stresses, the resulting residual stresses due to the overload should be independent of the time they occur. At the beginning, it should lead to identical residual stresses as after one transit, because every time the same cyclically stabilized stress-strain behavior is used. In Figure 11, however, it can be observed that the calculated mean stresses differ ( $\sigma_{m,num,start} = 103$  MPa vs.  $\sigma_{m,num,transit} = 67$  MPa). These differences are due to control inaccuracy in the fatigue test (it should be noted that in both variants the measured strains from the fatigue test were used for the fatigue assessments). In the scenario with the overload after one transit, an overshoot of the controlled strains occurred directly after the overload, which led to a reduction of the tensile residual stresses. This is shown in Figure 12. So a direct comparison between the residual stresses for both scenarios, overload at the beginning and overload after one transit, cannot be performed, even for nominal identical strain amplitude levels. However, for the comparison of the impact of the transient material behavior, it is not necessary that the mean stresses are

exactly the same because the fatigue assessments are evaluated with regard to their damage sum and the damage sum takes the mean stress into account.

In Figure 12, a jump in the stress after the overload cycles can be observed. This is due to the fact that the overload cycle was run with a very low test frequency ( $f = 0.01$  Hz). At this low frequency, creep effects are already visible, which can be seen in a reduction of the maximum stress. The following load cycles are performed with a higher frequency ( $f = 8 - 20$  Hz) and show a clear increase of the maximum stress. The variation of the test frequency was performed to find a compromise between test duration and control accuracy. The test frequency was varied in a range where no significant influence was expected. However, Figure 3 and Figure 12 show an influence. Though there is no significant influence on the main findings, since the same test frequencies were used for all scenarios, they are again comparable.

### 3.3 | Results of the fatigue assessments

In the damage accumulation, higher mean stresses lead to higher damage fractions due to the mean stress sensitivity of the material. In the calculations, the influence of the mean stresses on the fatigue damage are assessed in the damage parameter according to Bergmann and are weighted with the parameter  $k$ .

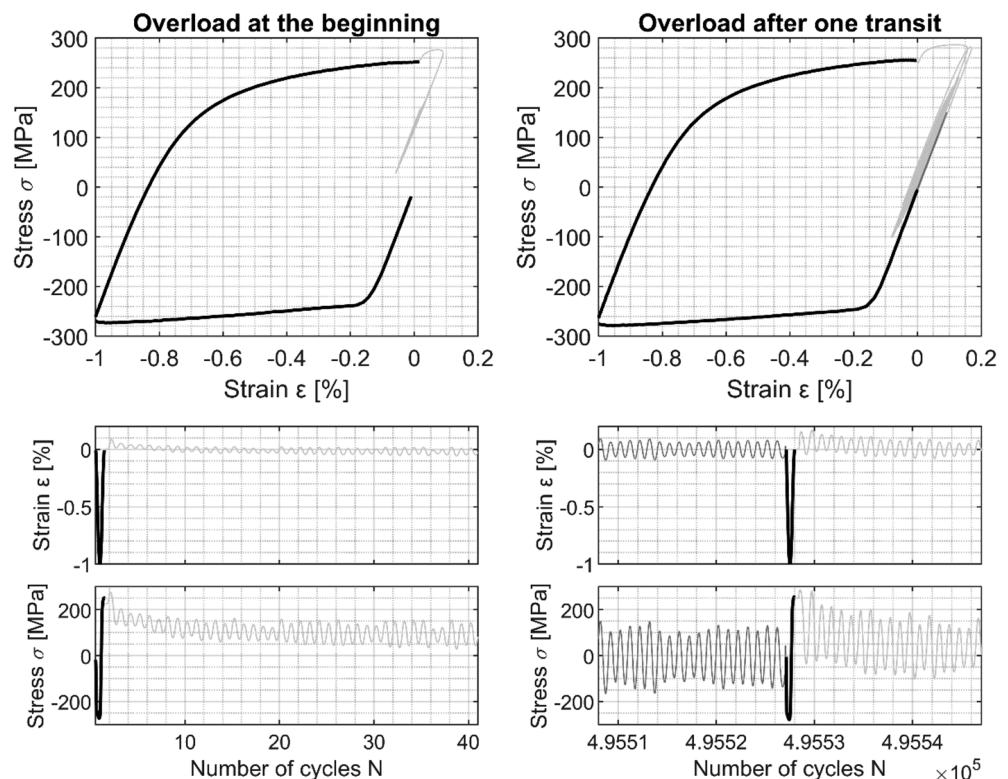


FIGURE 12 Measured stress-strain hystereses of overload cycles

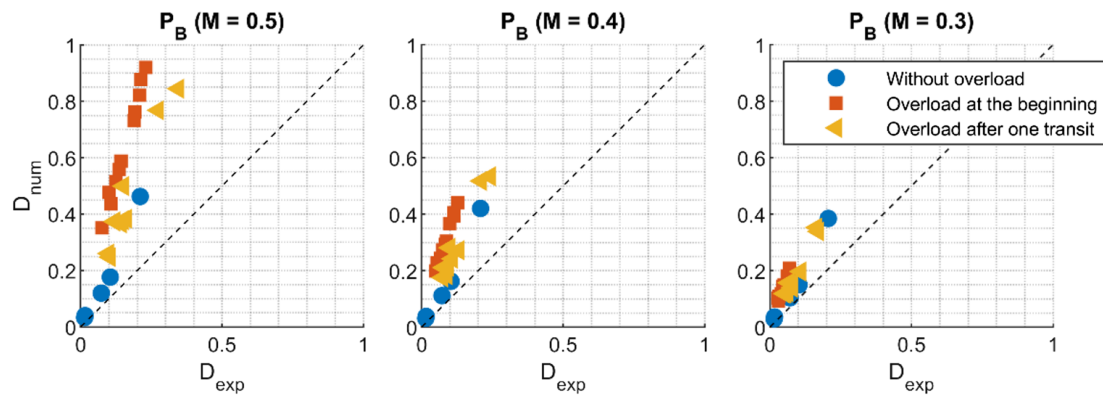


FIGURE 13 Correlation between damage sums derived using transient ( $D_{exp}$ ) and cyclically stabilized material behavior ( $D_{num}$ ) [Colour figure can be viewed at wileyonlinelibrary.com]

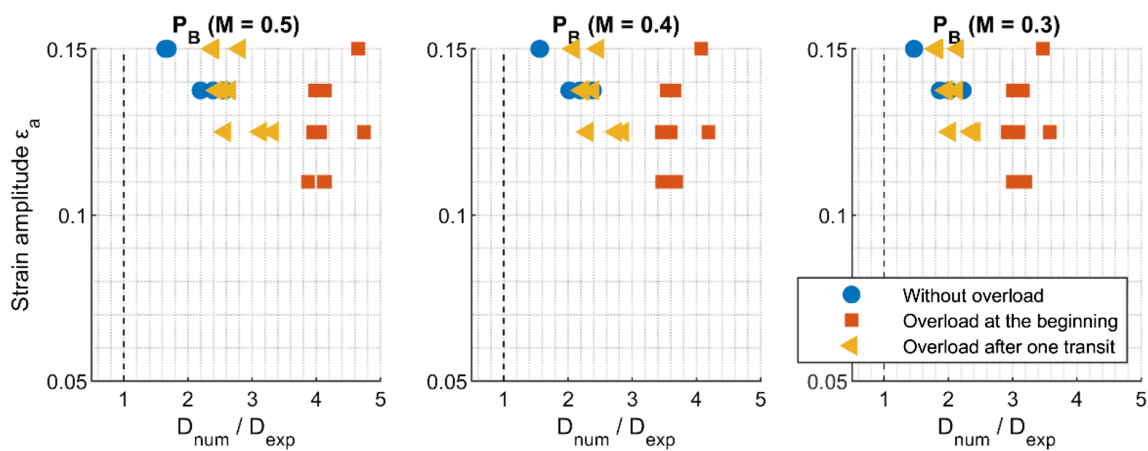


FIGURE 14 Impact of load level on the damage sum [Colour figure can be viewed at wileyonlinelibrary.com]

Since the mean stresses in the experimental variant are lower than in the numerical variant, the damage sums in the numerical variant are higher than those determined with transient material behavior (Figure 13). With increasing deviation of the mean stress between both variants, the deviation in the damage sums also increases. This is caused by a high mean stress sensitivity. Figure 14 shows that with increasing mean stress sensitivity, the damage sums of the different overload scenarios also deviate from each other. This indicates that a mean stress sensitivity of  $M = 0.3$  represents the different overload scenarios best, because there the smallest deviations between the damage sums of the overload scenarios are archived. The damage sum is not strongly depending on the mean stress or the occurrence of an overload; all fatigue tests fail at almost the same damage sum.

The calculated damage sums are in both cases clearly below the theoretical damage sum of  $D = 1$ , even if the transient material behavior with the measured stress amplitudes and mean stresses from the fatigue tests are taken into account (Figure 13). A dependence of the load

level on the damage sum could not be determined (Figure 14).

The derived damage sums are depending on the overload scenario and the mean stress sensitivity. In the numerical variant, the average damage sums lie between  $D = 0.2$  (without overload) and  $D = 0.6$  (overload at the beginning with a mean stress sensitivity of  $M = 0.5$ ). In the transient variant, the average damage sum lies between  $D = 0.06$  (without overload) and  $D = 0.2$  (overload after one transit with a mean stress sensitivity of  $M = 0.5$ ). In literature, allowable damage sums for nodular cast iron vary. Most recommendations<sup>39–41</sup> are between  $D = 0.2$  and  $D = 0.5$ ; however, recommendations<sup>4</sup> are also given with  $D = 1$ .

## 4 | SUMMARY AND CONCLUSIONS

In this paper, the influence of the transient material behavior on the damage sum in thick-walled nodular cast

iron was investigated. For this purpose, strain-controlled tests were performed under constant and variable strain amplitudes on specimens made of EN-GJS-400-18-LT. To investigate the influence of an overload, three overload scenarios were investigated—(a) without overload, (b) with an overload at the beginning, and (c) with an overload after one transit. The overload with  $\Delta\epsilon = 1\%$  and  $R = -\infty$  was applied only once in the overall test and has the aim of generating high tensile residual stresses. On the basis of the measured strains in the fatigue test, damage calculations were carried out using the strain-life approach. On one hand, characteristic damage sums for the material could be determined. On the other hand, the suitability of the strain-life approach for the assessment of overloads could be examined. In a further fatigue assessment, the influence of the transient material behavior on the damage sum has been determined. In this assessment the cyclic hardening, the mean stress relaxation and the creep of the material were considered. The investigations show that

- The conventional damage calculation with a simplified material behavior (w/o transient effects) leading to damage sums of about  $D = 0.2$  matches to the damage sums which can be found in literature
- The conventional damage calculation with a simplified material behavior (w/o transient effects) can be used to archive reliable results even if the materials show significant cyclic hardening and mean stress relaxation like EN-GJS-400 U-LT
- The conventional damage calculation with a simplified material behavior (w/o transient effects) leads to damage sums which are by a factor of 3 higher than those calculated by means of real transient material behavior. Therefore, it is important not to mix the variants. The determined endurable damage sum is always connected to the evaluation approach (e.g., transient or stabilized material behavior, damage parameter, and mean stress sensitivity). A combination of different approaches or boundary conditions may lead to non-conservative results.
- A mean stress sensitivity of  $M = 0.3$  represents the different overload scenarios best. The damage of the overload is essentially caused by the resulting tensile residual stresses.
- High load peaks within the load spectrum can lead to a reduction of the residual stresses, which is why the influence of the overload at high loads is lower than at lower load collectives.
- The use of a realistic transient material behavior does not necessarily lead to the theoretical damage sum of  $D_{th} = 1$ .

## ACKNOWLEDGMENTS

The results presented in this paper were derived in the project “GaßnerWind.” The authors thank the German Federal Ministry of Economics Affairs and Energy (BMWi) under the grant “0325707” for funding this project and the companies supporting the investigations.

Open Access funding enabled and organized by Projekt DEAL

## DATA AVAILABILITY STATEMENT

Data is available on request from the authors.

## NOMENCLATURE

$c$	fatigue ductility exponent
$b$	fatigue strength exponent
$f$	frequency
$h$	cyclic hardening
$k$	mean stress parameter
$n$	cyclic hardening exponent
$t$	time
$E$	Young's modulus
$K'$	cyclic hardening coefficient
$HBV_{90\%}$	highly stressed volume 90%
$L_s$	spectrum length
$M$	mean stress sensitivity
$N$	number of cycles
$N_i$	number of cycles to crack initiation
$P_B$	damage parameter according to Bergmann
$R_e$	strain ratio
$\epsilon$	strain
$\epsilon_a$	strain amplitude
$\epsilon_{a,e}$	elastic strain amplitude
$\epsilon_{a,p}$	plastic strain amplitude
$\epsilon'_f$	fatigue ductility exponent
$\Delta\epsilon$	strain range
$\sigma$	stress
$\sigma_a$	stress amplitude
$\sigma_m$	mean stress
$\sigma'_f$	fatigue strength coefficient

## ORCID

Jörg Baumgartner  <https://orcid.org/0000-0002-0225-275X>

## REFERENCES

1. IEC 61400-1. Wind turbines—part 1: design requirements, 2019.
2. Fatemi A, Yang L. Cumulative fatigue damage and life prediction theories: a survey of the state of the art for homogenous materials. *Int J Fatigue*. 1998;20(1):9-34. [https://doi.org/10.1016/S0142-1123\(97\)00081-9](https://doi.org/10.1016/S0142-1123(97)00081-9)
3. ST-0361: Machinery for wind turbines.

4. Rennert R, Kullig E, Vormwald M, Esderts A, Luke M. FKM guideline—analytical strength assessment of components, 2020.
5. Dowling NE, Brose WR, Wilson WK. Notched member fatigue life predictions by the local strain approach. In: *Fatigue Under Complex Loading—Analysis and Experiment*. SAE; 1977:55-84.
6. Fiedler M, Wächter M, Varfolomeev I, Vormwald M, Esderts A. Rechnerischer Festigkeitsnachweis unter expliziter Erfassung nichtlinearen Werkstoffverformungsverhaltens (engl.: FKM Guideline on the fatigue assessment under explicit consideration of the nonlinear material behaviour). VDMA, 2019.
7. Sonsino CM, Kaufmann H, Wagener R, Fischer C, Eufinger J. Interpretation of overload effects under spectrum loading of welded high-strength steel joints. *Weld Int*. 2011;55(11-12): 66-78. <https://doi.org/10.1007/BF03321544>
8. Baumgartner J, Bruder T. Influence of weld geometry and residual stresses on the fatigue strength of longitudinal stiffeners. *Weld Int*. 2013;6(6):841-855. <https://doi.org/10.1007/s40194-013-0078-7>
9. Yin F, Fatemi A, Bonnen J. Variable amplitude fatigue behavior and life predictions of case-hardened steels. *Int J Fatigue*. 2010;7(7):1126-1135. <https://doi.org/10.1016/j.ijfatigue.2009.12.009>
10. Mottitschka T, Pusch G, Biermann H, Zybelle L, Kuna M. Influence of overloads on the fatigue crack growth in nodular cast iron: experiments and numerical simulation. *Proc Eng*. 2010; 2(1):1557-1567.
11. Morrow J, Ross AS, Sinclair GM. Relaxation of residual stresses due to fatigue loading. *SAE Trans*. 1960;40-48.
12. Martinsson A, Andersson-Östling HCM. Creep testing of nodular iron at ambient and elevated temperatures. Swerea KIMAB AB. 2010.
13. Jiang Y, Sehitoğlu H. Modeling of cyclic ratchetting plasticity, part II: comparison of model simulations with experiments. *J Appl Mech*. 1996;3(3):726-733. <https://doi.org/10.1115/1.2823356>
14. Heinrietz A, Hessler J. An approach for the fatigue estimation of porous cast iron based on non-destructive testing results. MATEC Web of Conferences. 2014;12:05001 <https://doi.org/10.1051/mateconf/20141205001>
15. Bleicher C, Wagener R, Kaufmann H, et al. Assessment of the fatigue strength of thick-walled nodular cast iron with Dross. *Proc Struct Integr*. 2019;18:46-62. <https://doi.org/10.1016/j.prostr.2019.08.139>
16. Bergner K, Hessler J, Bleicher C. Fatigue analysis of cast iron components considering the influence of casting skin. *Proc Struct Integr*. 2019;19:140-149. <https://doi.org/10.1016/j.prostr.2019.12.017>
17. Bleicher C, Wagener R, Kaufmann H, Melz T. Fatigue assessment of nodular cast iron with material imperfections. *SAE Int J Engines*. 2017;10(2):340-349. <https://doi.org/10.4271/2017-01-0344>
18. Borsato T, Ferro P, Berto F. Novel method for the fatigue strength assessment of heavy sections made by ductile cast iron in presence of solidification defects. *Fatigue Fract Eng Mater Struct*. 2018;4(8):1746-1757. <https://doi.org/10.1111/ffe.12815>
19. Čanžar P, Tonković Z, Drvar N, Bakić A, Kodvanj J, Sorić J. Experimental investigation and modelling of fatigue behaviour of nodular cast iron for wind turbine applications. Proceedings of the 8th International Conference on Structural Dynamics, EURO-DYN. 2011.
20. Bleicher C, Kaufmann H, Melz T. Assessment of service loads and material influence on the lifetime of thick-walled nodular cast iron components. *Int J Fatigue*. 2021;6:106171. <https://doi.org/10.1016/j.ijfatigue.2021.106171>
21. Bleicher C, Wagener R, Kaufmann H. *Fatigue Behavior of Large Cast Components Under Variable Amplitude Loading with Overloads*. SAE World Congress Experience, Detroit. 2019. <https://doi.org/10.4271/2019-01-0526>
22. Kuguel R. A relation between theoretical stress concentration factor and fatigue notch factor deduced from the concept of highly stressed volume. Sixty-fourth Annual Meeting of the Society (ASTM), June 25–30, 1961: 732–744.
23. Sonsino CM. Zur Bewertung des Schwingfestigkeitsverhaltens von Bauteilen mit Hilfe örtlicher Beanspruchungen (engl.: On the fatigue assessment of components on the basis of local stresses). *Konstruktion*. 1993;1:25-33.
24. ISO 12106:2017 Metallic materials — Fatigue testing — Axial-strain-controlled method, 2017.
25. Ramberg W, Osgood WR. Description of stress-strain curves by three parameters. NACA Technical Notes No. 902, 1943.
26. Coffin LF. A study of the effects of cyclic thermal stresses on a ductile metal. 1954: 931–981.
27. Manson SS. Fatigue: a complex subject—some simple approximations. *Exp Mech*. 1965;5(4):193-226.
28. Basquin OH. The exponential law of endurance tests. Proceedings of American Society of Testing Materials 1910.
29. Morrow JD. Cyclic plastic strain energy and fatigue of metals. *ASTM STP*. 1965;378:45-87.
30. Haibach E. *Betriebsfestigkeit: Verfahren und Daten zur Bauteilberechnung (engl. Structural Durability: Procedures and Data for the Assessment of Components)*. 3rd ed. Springer VDI; 2006.
31. Sonsino CM. Fatigue testing under variable amplitude loading. *Int J Fatigue*. 2007;6(6):1080-1089. <https://doi.org/10.1016/j.ijfatigue.2006.10.011>
32. Masing G. Eigenspannung und Verfestigung beim Messing. Proceeding of the 2nd International Congress for Applied Mechanics, Zürich, Switzerland, 1926: 332–335.
33. Clormann U, Seeger T. RAINFLOW - HCM Ein Zählverfahren für Betriebsfestigkeitsnachweise auf werkstoffmechanischer Grundlage (engl.: RAINFLOW - HCM A counting algorithm for the fatigue strength assessment based on material mechanics). *Stahlbau*. 1986;3:65-71.
34. Bergmann J. Zur Betriebsfestigkeitsbemessung gekerbter Bauteile auf der Grundlage der örtlichen Beanspruchungen (engl. A contribution to the fatigue strength assessment of notched components based on local stresses). PhD-Thesis. Institut für Stahlbau und Werkstoffmechanik, 1983.
35. Smith KN, Watson P, Topper TH. A stress-strain functions for the fatigue on materials. *J Mater*. 1970;5:767-778.
36. Bleicher C, Wagener R, Kaufmann H, Melz T. Fatigue strength of nodular cast iron with regard to heavy-wall applications. *Mater Test*. 2015;9:723-731.
37. Palmgren A. Die Lebensdauer von Kugellagern. *VDI-Z*. 1924; 339-341.
38. Miner MA. Cumulative damage in fatigue. *J Appl Mech*. 1945; 12:159-164.



39. Kaufmann H. Zur schwingfesten Bemessung dickwandiger Bauteile aus GGG-40 unter Berücksichtigung von gießtechnisch bedingter Gefügeungängen (engl. A contribution to the design of thick walled components made from GGG-40 under consideration of casting related inhomogeneities), Fraunhofer Report FB-214, 1998.
40. Schönborn S, Kaufmann H, Sonsino CM, Heim R. Variable amplitude fatigue of high-strength cast iron alloys for automotive applications. *Int J Fatigue*. 2016;10:445-458. <https://doi.org/10.1016/j.ijfatigue.2016.01.006>
41. Sonsino CM, Kaufmann H, Engels A. Schwingfestigkeit von randschichtnachbehandelten duktilen Gußeisenwerkstoffen unter konstanten und zufallsartigen Belastungen (engl.: Fatigue

strength of surface treated ductil cast iron under constant and variable amplitude loading). *Konstruieren Gießen*. 1999;4:4-16.

**How to cite this article:** Hesseler J, Baumgartner J, Bleicher C. Consideration of the transient material behavior under variable amplitude loading in the fatigue assessment of nodular cast iron using the strain-life approach. *Fatigue Fract Eng Mater Struct*. 2021;44(10):2845–2857. <https://doi.org/10.1111/ffe.13519>